Organic & Biomolecular Chemistry

Accepted Manuscript

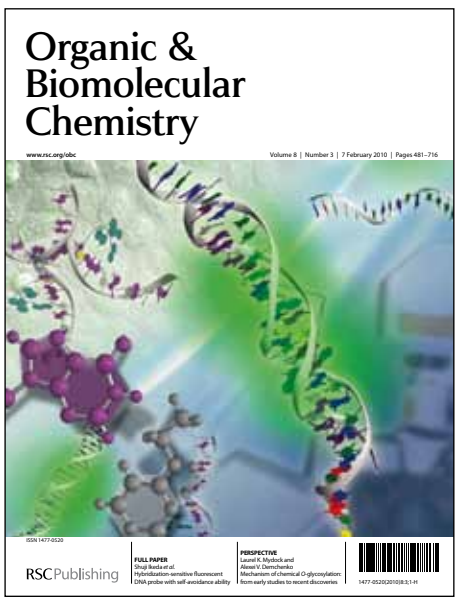

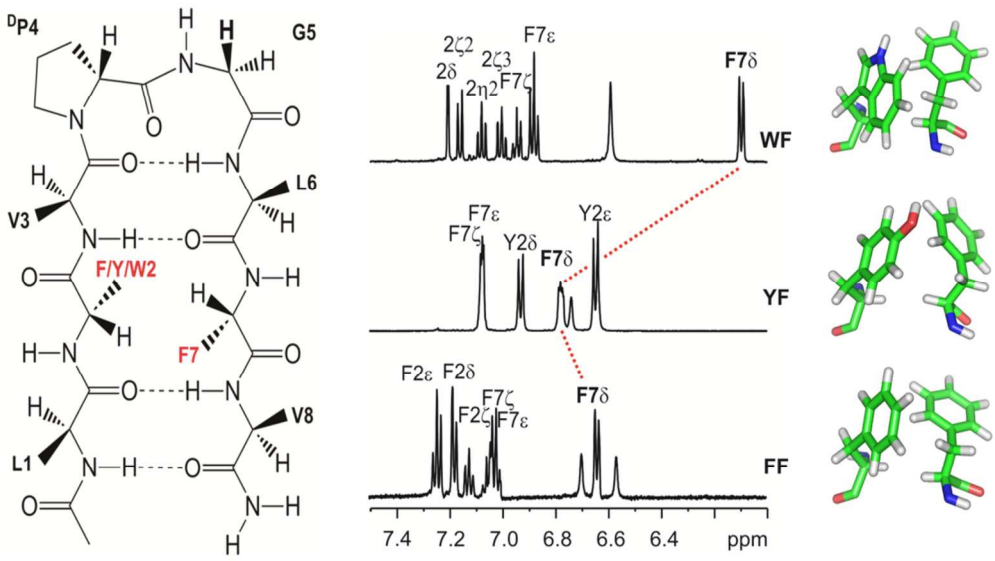

Examination of the preferential interaction geometries of the aromatic amino acids Phe, Tyr and Trp with the benzyl ring of Phe in designed octapeptide hairpin scaffolds reveals stabilizing contributions of a Trp-Phe pair, even in amphipathic solvents.

Cite this: DOI: 10.1039/c0xx00000x

www.rsc.org/xxxxxx

ARTICLE TYPE

Comparative analysis of cross strand aromatic-Phe interactions in designed peptide β-hairpins

Kamlesh Madhusudan Makwana[a] and Radhakrishnan Mahalakshmi*[a]

Received (in XXX, XXX) Xth XXXXXXXXX 20XX, Accepted Xth XXXXXXXXX 20XX

DOI: 10.1039/b000000x

The mode(s), geometry and strength of interaction of the three aromatic amino acids, namely Phe, Tyr and Trp, with the benzyl side chain of Phe, at the non-hydrogen bonding position of designed model octapeptide β-hairpins, nucleated by the central ^{D}Pro-Gly turn, have been examined. In the absence of solvent-driven hydrophobic forces, the extent of contribution of such interactions indicates that the stereospecific face-to-edge (FtE) geometry of aromatic rings is most stabilizing in the Trp-Phe pair. In contrast, our study shows that the Tyr-Phe pair exhibits the weakest interaction energy, despite its abundance in protein structures. The contribution of aromatic interactions as opposed to the influence of spatial proximity to electron-rich groups, to the observed anomalous backbone and side chain chemical shifts, has also been delineated. Our findings indicate that the Trp-Phe pair contributes an additional ~0.9 kcal/mol and ~1.3 kcal/mol towards scaffold stabilization, when compared with the Phe-Phe and Tyr-Phe pair, respectively, even in an amphipathic solvent such as methanol. Detailed NMR analysis of backbone resonances, as well as the extent of pronounced anomalous chemical shifts, indicates that the strength of aromatic interactions with Phe follows the order Trp>Phe>Tyr. Furthermore, the advantages of Trp-Phe or Phe-Phe pairs as alternative structure stabilizing elements are also highlighted.

Introduction

Favourable long-range interactions involving amino acid side chains are widely accepted contributors to the stability of isolated α-helical[1] and β-sheet structures.[2] In particular, aromatic interactions enhance the structure and folded populations of β-hairpins when they are situated at the non-hydrogen bonding position of strand segments.[2c, 2h, 3] A study has indeed demonstrated that in aqueous media, side-chain interactions between strategically positioned Trp-Trp pairs at the non-hydrogen bonding position are superior β-sheet stabilizing agents than the disulphide bond.[4] On the contrary, placement of aromatic residues at the hydrogen bonding site destabilizes the β-hairpin.[3h] Previous surveys have reported that aromatic dimers prefer favourable T-shaped interactions, while stacked or parallel displaced geometries can also play competitive roles, depending on solvent polarity and hydrogen bonding.[5] In the gas phase, benzene dimers display multiple geometries that can broadly be categorized under stacked, displaced and T-shaped arrangements.[5a, 6] Aromatic interactions examined thus far therefore demonstrate strong preferences for geometry and directionality.

In proteins, aromatic dimers show surprisingly more stability in a displaced π-stacking manner, as opposed to the more popular T-shaped geometry.[7] The significance of such aromatic interactions in secondary structure stabilization in proteins and isolated peptide sequences is well recognized. However, the geometries of association, and the accompanying contribution to the folding free energy, are not extensively enumerated, as they are usually convoluted by several factors. Primarily, the preponderance of aromatic clusters[5b] in the protein hydrophobic core precludes accurate determination of contributions that arise from a single interacting pair of aromatic side chains. In addition, such interaction geometries are heavily influenced by overwhelming contributions of other stabilizing interactions, such as salt bridges and hydrogen bonds. Peptide systems that can adopt pre-nucleated scaffolds are often considered excellent systems for addressing stereospecific interactions in isolation.[6a] Such peptides have largely been examined in aqueous environments, wherein solvent-driven hydrophobic interactions and entropic effects are predominant driving factors between aromatic side chains.[8] In less polar solvents, several studies have exploited Phe-Phe interactions as β-hairpin stabilizing agents in synthetic model peptides.[2f, 2h, 9] NMR and X-ray studies have established that T-shaped interactions are the preferred geometries for stabilizing Phe-Phe pairs in organic solvents.[6b, 9a, 10]

A survey of possible isolated aromatic dimers observed in protein structures revealed that the most abundant interaction occurs between Phe-Tyr pairs.[5b] This is closely followed by Phe-Phe pairs, and the occurrence of Phe-Trp pairs is ~50% of Phe-Tyr interactions. Tyrosine, being slightly hydrophilic in nature, has an interestingly greater percentage of aromatic dimers than the more hydrophobic Phe-Phe or Phe-Trp clusters.[5b] Phenylalanine, in particular, may be considered the most apolar

Peptide Code	Sequence	Schematic
FF	Ac-L-F-V-^{D}P H_2N-V-F-L-G	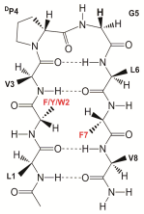
YF	Ac-L-Y-V-^{D}P H_2N-V-F-L-G	
WF	Ac-L-W-V-^{D}P H_2N-V-F-L-G	

Fig. 1 Designed model octapeptide sequences examined in this study along with a schematic representation of the β-hairpins **FF**, **YF** and **WF**. The non-hydrogen bonding position, which allows for close proximity of the aromatic rings, is highlighted in red.

of the three aromatic residues, due to the lack of polar groups such as OH and NH, which are present in Tyr and Trp, respectively. Not surprisingly, Phe scores the highest, among the aromatic amino acids, in the different hydrophobicity scales, including Kyte and Doolittle,[11] Wolfenden,[12] and Janin,[13] suggesting that the greatest solvophobic effect in water would be experienced by the benzyl ring. Hence, in order to understand preferential interactions between aromatic side chains and phenylalanine, one may consider the use of a medium that does not specifically drive hydrophobic interactions. Polar amphipathic solvents, such as methanol,[14] serve as excellent choices to systematically compare aromatic-Phe interactions in designed secondary structure scaffolds. In this study, we address the preferential modes of interaction between specific pairs of aromatic side chains involving phenylalanine, the impact of such an interacting aromatic dimer on local structural stability and geometries as well as favoured modes of interaction.

Results and Discussion

Scaffold design and choice of sequence elements

Octapeptide sequences described in this study were designed based on previous reports of successful β-hairpin scaffolds synthesized to probe cross-strand interactions.[2h, 6b, 9a, 15] Dipeptide segments adopting type I'/II' turn have been extensively used to nucleate β-hairpin scaffolds for the examination of cross-strand aromatic interactions, especially with facing Phe pairs at the non-hydrogen bonding position.[2h, 9b, 15] A recent study which compared crystal structures of eight octapeptide hairpins nucleated by different turn segments revealed that the shortest centroid-to-centroid distance for a ^{D}Pro-Gly nucleated hairpin.[9a] Hence, we chose the ^{D}Pro-Gly unit as the turn nucleating element for our sequences. Furthermore, this would allow for comparison of our results with earlier reports. Different molecular conformations of short peptide segments have previously been observed upon changing the N-terminal protecting group. For example, crystal structures of the tripeptides Boc-L-W-V-OCH_3 and Ac-L-W-V-OCH_3 (Boc = *t*-butyloxycarbonyl; Ac = acetyl) revealed a folded β-turn structure for the former and an extended conformation for the latter.[16] We therefore acetylated the N-terminus of all the peptides, so as to achieve extended strand segments. Based on the model octapeptide β-hairpins, peptides **FF**, **YF** and **WF** were generated (Fig. 1). The residue at position 2 was systematically substituted with the three aromatic amino acids, which allowed for comparison of aromatic-Phe interactions.

Conformational features of the Aro-Phe peptide backbone

All peptides were highly soluble in methanol, and displayed sharp well-resolved resonances (Fig. S1-S2 in Electronic Supplementary Information, ESI†). Complete backbone and side chain assignments were obtained by NMR spectroscopy using a combination of homonuclear ^{1}H-^{1}H TOCSY and ROESY experiments. In the ROESY spectra all three peptides exhibited weak self $d_{N\alpha}$ NOEs and strong sequential $d_{\alpha N}$ NOEs for residues 1-3 and 6-8 (Fig. S3†), which are expected to constitute the hairpin arms. Observation of these NOEs indicated that, by and large, these regions adopted the extended conformation. The presence of a *trans* peptide unit at the Val3-^{D}Pro4 segment was confirmed by the observation of a strong $3^{\alpha}H\leftrightarrow4^{\delta}H$ NOE in all peptides. Furthermore, evidence for turn nucleation was obtained from presence of the Gly5 NH↔Leu6 NH resonance. Finally, existence of a well-folded target β-hairpin scaffold and strand registry in all three peptides was established using the diagnostic backbone Phe/Tyr/Trp2 $C^{\alpha}H\leftrightarrow$Phe7 $C^{\alpha}H$ NOE, and the d_{NN} NOEs between Val3 NH↔Leu6 NH and Leu1 NH↔Val8 NH (Fig. 2). A weak 1NH↔2NH NOE was also observed in all three peptides, suggesting that some strand fraying occurred towards the N-terminus. Such strand fraying at the termini is typical in designed β-hairpins, and has been observed earlier.[3c] However, we also observe the rather unusual $2C^{\alpha}H\leftrightarrow$8NH NOE in all three peptides (Fig. S3†), which supports strand registry.[2h, 17] The distance between these two protons is greater than the 1NH↔8NH distance in a folded octapeptide hairpin; despite this, a strong NOE is observed between $2C^{\alpha}H\leftrightarrow$8NH, indicating that backbone conformational flexibility is restricted to ϕ and ψ of Leu1. Additionally, we probed the temperature dependence of the backbone amide chemical shifts and calculated the corresponding dδ/dT values (Fig. S4†). Higher dδ/dT values observed for the 2nd, 5th and 7th NH indicate solvent exposed amides, while the other NH resonances show lower dδ/dT values, suggestive of internally hydrogen bonded amides, as reported earlier in similar peptide systems.[2h, 9] However, in short peptide hairpins, these dδ/dT values must be interpreted with caution.[18]

Aromatic pair influences the extent of β-hairpin formation

Dispersion of backbone resonances (NH and $C^{\alpha}H$) and chemical shift indexing (CSI) are known to corroborate with the extent of folding in β-hairpin peptides.[2b] A close observation of the ^{1}H 1D spectra for all three peptides (Fig. S1-S2†) indicates a marginally greater dispersion of amide resonances and downfield shifted $C^{\alpha}H$ chemical shifts for **WF**, while **FF** and **YF** show comparable dispersions. This is also reflected in the calculated CSI (Fig. 3A), in which the overall values are higher for **WF**. Likewise, an increase in separation between the geminal Gly $C^{\alpha}H$ chemical shifts is also an indicator of turn geometry.[2b, 19] We observe a high degree of geminal non-equivalence of the Gly $C^{\alpha}H$ resonances in the order **WF**>**FF**>**YF** (Fig. 3B), which is in good agreement with the CSI and folded fractions at 303K. The corresponding folding free energy, summarized in Fig. 3B, indicates that the Trp-Phe interaction contributes an additional favourable folding free energy of 0.93kcal/mol and 1.33kcal/mol over the Phe-Phe and Tyr-Phe interactions, respectively. This observation suggests greater precedence for folded peptide in **WF** and destabilization in **YF**, when compared with **FF** and **WF**.

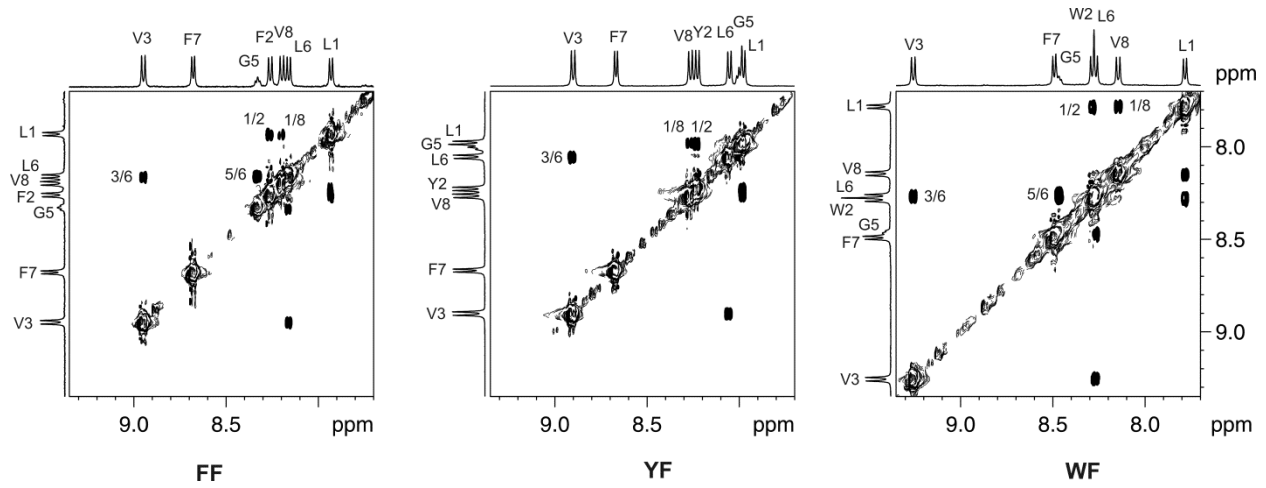

Fig. 2 Partial expansions of homonuclear ^{1}H-^{1}H NMR ROESY spectra of **FF**, **YF** and **WF**, in CD_3OH, highlighting diagnostic β-hairpin NH-NH NOEs.

We next translated the inter-proton NOEs observed in the ROESY spectra to distance restraints (Table S1†) in CYANA v2.1,[20] and determined the solution NMR structures in methanol. Superposition of the 35 best structures calculated for each peptide is illustrated in Fig. 3C and average backbone torsion angles are listed in Table S2†. The structures clearly indicate that aromatic ring substitution greatly influences the establishment and stabilization of favourable long-range backbone as well as side chain contacts, allowing for better refinement of the structure, and consequently resulting in lower RMSDs. This is evident in the calculated structure of **WF**.

An interesting deviation from the anticipated CSI values in **WF** is observed in the case of Trp2 (Fig. 3A and Fig. S5†). While the CSI values of the other $C^{\alpha}H$ protons are largest in this peptide, the Trp2 CSI is lowered. We therefore compared the phi values derived from the calculated structure and the $^{3}J_{NH\text{-}C^{\alpha}H}$, with the CSI (Table 1). Notably, the phi value for Trp2 in **WF** is ~ -99°, which is not in line with phi values obtained for **FF** and **YF**, and is significantly deviated from the ideal ϕ of -139° for antiparallel β-sheets, despite overwhelming evidence for highest hairpin population in **WF**. Conformations of tryptophan with sub-optimal phi geometry have also been observed earlier,[3a, 3g] and reflect the absence of a defined secondary structure propensity for this residue.[21] Despite this, the overall stability conferred by the indole ring supersedes the local distortion of the backbone, indicating that Trp residues lead to structural stability of β-hairpin scaffolds by establishing optimal tertiary contacts.

Aromatic ring orientations are face-to-edge and populate only one observable conformer in FF and WF

Structural studies of aromatic pairs in peptide β-hairpins have earlier observed that T-shaped edge-to-face (EtF) or face-to-edge (FtE) ring orientations are widely prevalent, with interplanar angles approaching 90°.[3a, 3g, 6b, 22] Additionally, in short peptides with a single pair of interacting aromatics, a preferential orientation of the N-terminal ring towards the turn leading to a FtE aromatic geometry is largely observed.[3a, 3e, 3g] In our peptides, the occurrence of such side chain orientation would necessarily place the Phe7 ring protons directly in the shielding zone of the F/Y/W2 ring. FtE geometries of Phe-Phe pairs in octapeptide hairpins are known to cause an upfield shift of Phe7 $C^{\delta}H$ from ~7.22ppm to 6.65-6.76ppm and an accompanying shift of $C^{\varepsilon/\zeta}H$ by ~0.15ppm, due to shielding.[9a] We observe an overall upfield shift of -0.55ppm ($C^{\delta}H$), -0.20ppm ($C^{\varepsilon}H$) and -0.13ppm ($C^{\zeta}H$), respectively, for the Phe7 ring protons of **FF**, which supports a T-shaped FtE geometry for Phe-Phe interactions, and suggests that the aromatic interactions in this peptide are possibly stronger than those observed earlier in similar peptides nucleated by non-^{D}PG turn.[9a] Furthermore, **YF** and **WF** also demonstrate a similar pattern of upfield shifted Phe7 ring resonances, indicating that the FtE geometry is universally conserved, and may be necessary to impart structural stability to the hairpin.[6b, 9a]

We further confirmed presence of the T-shaped geometry and aromatic ring positions using key NOEs observed for both the ring protons across the three peptides (Fig. S6† and Fig. S7†). The characteristic $2C^{\delta}H\leftrightarrow7C^{\alpha}H$, $2C^{\delta/\varepsilon}H\leftrightarrow7C^{\delta}H$, $2C^{\alpha}H\leftrightarrow7C^{\delta}H$ NOEs indicate cross-strand aromatic interactions in the peptide **FF**. NOEs between $2C^{\delta/\varepsilon}H\leftrightarrow3NH/5C^{\alpha}H/6NH$ and $7C^{\varepsilon}H$ to the acetyl group position the Phe2 and Phe7 rings towards the turn and termini, respectively. This is well in agreement with the observed ring orientations obtained from crystal and NMR structures for this peptide.[9a, 15a] A similar NOE pattern is observed in the case of **YF**, wherein medium to weak $2C^{\delta/\varepsilon}H\leftrightarrow7C^{\delta/\varepsilon/\zeta}H$ NOEs, along with $2C^{\alpha}H\leftrightarrow7C^{\delta}H$ and $2C^{\delta}H\leftrightarrow7C^{\alpha}H$, position the two rings in close spatial interaction.

The bulkiness of the indole ring allows it to establish favourable interactions with a larger number of backbone and side chain atoms. Hence, the **WF** spectrum is populated by stronger and larger number of NOEs between the Trp2 indole to Val3, Gly5 and Leu6, positioning the indole ring orientation towards the turn segment (Fig. S6†). NOEs observed between Phe7 $C^{\varepsilon/\zeta}H$ to Leu1 NH and the acetyl- and -$CONH_2$ groups at the termini, allows for positioning of this side chain. In addition, we observe NOEs between $2N^{\varepsilon1}H\leftrightarrow7C^{\delta}H$, $2C^{\alpha}H\leftrightarrow7C^{\delta}H$, $2C^{\delta}H\leftrightarrow7C^{\delta}H$, which support a proper T-shaped geometry for the rings, in which $7C^{\delta}H$ protons and $7C^{\beta}H$ protons fall directly under the shielding zone of the penta- and hexa- rings of tryptophan, respectively (Fig. S6† and Fig. S7†). All three peptides therefore exhibit a FtE geometry between the aromatic rings, with F/Y/W2 oriented towards the turn, and F7 towards the termini.

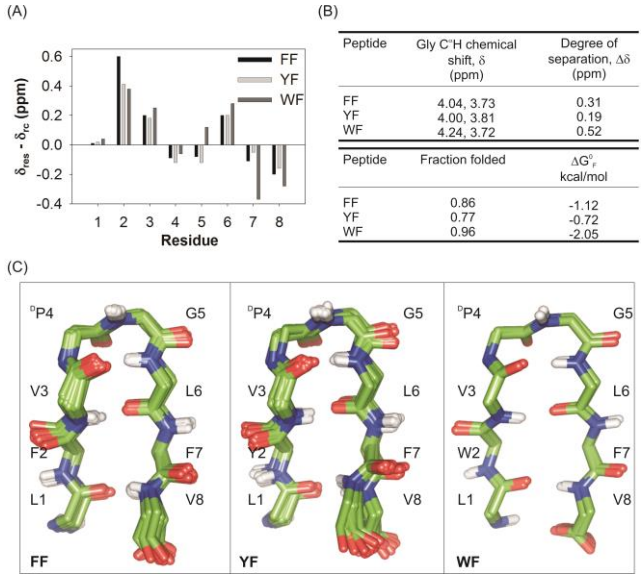

Fig. 3 Comparison of the extent of folding and NMR derived solution structures of **FF**, **YF** and **WF**. (A) Chemical shift indexing (CSI) calculated using $C^{\alpha}H$ shifts for the three peptides. The observed anomalous values for Phe7 and Val8 are due to the influence of ring currents, which is strongest in **WF**. (B) (Top) Comparison of the extent of geminal non-equivalence of Gly5 $C^{\alpha}H$. (Bottom) Folded populations and free energy of folding (ΔG^0_F) calculated using chemical shifts for the three peptides. (C) Superposition of 35 best structures calculated using NOEs obtained from ROESY spectra of the peptides in CD_3OH. Mean backbone RMSDs for **FF** = 0.22 +/- 0.14 Å, **YF** = 0.35 +/- 0.24 Å, **WF** = 0.01 +/- 0.02 Å. Mean global heavy atom RMSDs for **FF** = 0.71 +/- 0.22 Å, **YF** = 0.88 +/- 0.29 Å, **WF** = 0.16 +/- 0.15 Å.

Table 1 Comparison of $^3J_{NH\text{-}C^{\alpha}H}$, phi and psi values across the peptides

Peptide	Param-eter[a]	Leu1	Phe/Tyr/ Trp2	Val3	Leu6	Phe7	Val8
FF	$^3J_{NH\text{-}C^{\alpha}H}$	8.34	9.18	9.45	8.84	7.79	9.59
	ϕ	-	-126	-136	-133	-130	-130
	ψ	76	137	73	157	142	-
YF	$^3J_{NH\text{-}C^{\alpha}H}$	8.17	9.19	9.58	8.90	7.88	9.63
	ϕ	-	-130	-136	-128	-130	-130
	ψ	81	143	73	169	148	-
WF	$^3J_{NH\text{-}C^{\alpha}H}$	8.51	9.21	9.71	9.50	8.24	9.75
	ϕ	-	-99	-126	-128	-119	-140
	ψ	85	126	75	142	144	-

[a] Coupling constants ($^3J_{NH\text{-}C^{\alpha}H}$) were measured from ^1H 1D spectra. Φ-ψ values were obtained from the mean of 35 best structures (see Table S2).

The crystal structures of several octapeptide hairpins with Phe-Phe interactions suggested the existence of both T-shaped and inclined geometries (~45° interplanar angles).[6b] An intriguing possibility is the existence of such displaced geometries for aromatic interactions, which would position ring protons of both the aromatic residues in close proximity so as to cause shielding of certain aromatic resonances of *both* the interacting rings. However, the observed chemical shifts of aromatic resonances (listed in Fig. S1-S2†) do not reveal noticeable upfield shifts for F/Y/W2; instead, these ring protons (with the exception of Trp2 $C^{\varepsilon 3}H$ in **WF**) show a marginal downfield shift with change in temperature (see Fig. 5, described later), suggesting that the inclined geometry is less likely to occur in these sequences in solution, under the conditions examined.[9b]

Alternative ring orientations, giving rise to two conformers (I and II), have been earlier observed between Phe pairs in octapeptide β-hairpins.[6b, 9b] We therefore examined the occurrence of multiple conformers in our peptides by comparing the observed NOE pattern to that reported earlier.[9b] In **FF** and **WF**, all the observed long-range NOEs can readily be accounted for, if we were to consider a single conformer, corresponding to the previously reported conformer I of the peptide Boc-LFV-^{D}P^{L}P-LFV-OCH_3.[6b, 9b] The characteristic NOEs that define conformer II are not detectable in **FF** and **WF** spectra. However, in **YF**, the $2C^{\beta}H \leftrightarrow 7C^{\varepsilon/\zeta}H$, $2C^{\delta/\varepsilon}H \leftrightarrow 4C^{\beta/\gamma/\delta}H$ NOEs, assigned previously to conformer II,[9b] are observable (Fig. S8†), although the NOE is weak. It is therefore likely that Tyr-Phe interaction in methanol supports two alternative ring orientations. Indeed, in the **YF** spectrum (Fig. S1b†; also see Fig. 4B), $7C^{\delta}H$ splitting pattern resembles two closely resonating doublets; we speculate that this may arise from dual occupancy of the Phe7 ring.

Overall, we observe that the only ring orientations with sufficient occupancy, and are thereby stable enough for observation under NMR chemical shift timescales, are concurrent with T-shaped ring geometries. No alternative local minima seem to exist for **FF** and **WF**, in our experiments.

Influence of the proximal aromatic partner on Phe7 benzyl ring reflects interaction strengths

The presence of ring currents is known to influence NMR parameters of spatially proximal resonances.[3a, 9a] In the FtE geometry, the strength of aromatic interactions can be assessed from the extent of upfield shifted resonances of the ring which constitutes the 'edge' in the interacting pair.[2h] This is evident in Fig. 4A, wherein we compare the observed chemical shifts of Phe2 and Phe7 ring protons of **FF**, with the reported chemical shifts of control peptides lacking proximal aromatic interactions, namely (i) Boc-L-F-V-OCH_3[9b] and (ii) Boc-LVV-^{D}PG-LFV-OCH_3[9b]. The Phe7 $C^{\delta}H$ resonances of **FF** are upfield shifted, when compared with peptides (i) and (ii),[9b] indicating that proximal aromatic interactions lead to anomalous chemical shifts. Now, when we assess the strength of aromatic interactions between **FF**, **YF** and **WF** (Fig. 4B), the $7C^{\delta}H$ chemical shift is dramatically affected with change in ring substitution at position 2. The magnitude of upfield shift in $7C^{\delta}H$, with respect to peptide (ii)[9b] chemical shift of 7.205ppm as control, are: -0.525ppm (**FF**), -0.405ppm (**YF**) and -1.055ppm (**WF**) The strongest influence is observed in **WF**, in agreement with the highest stability displayed by this sequence. The interaction strength follows the order **WF**>**FF**>**YF**, unlike the anticipated **WF**>**YF**>**FF** if the observed $7C^{\delta}H$ pattern were arise exclusively due to the electron density within the interacting aromatic pair. Interestingly, replacement of the benzyl with a phenolic ring (Phe→Tyr substitution in **YF**) does not provide a proportionate upfield shift of the $7C^{\delta}H$. Instead, this resonance is less affected by the proximal electron cloud of tyrosine, suggestive of weaker aromatic interactions.

Aromatic shielding also affects the chemical shift dispersion of Phe7 resonances.[9b] In **YF**, this dispersion is greatly reduced, with clustering of $7C^{\varepsilon}H$ and $7C^{\zeta}H$ chemical shifts, while these resonances are well separated in **WF**. The features that are immediately evident from this comparison are (i) the extent of shielding is greatest in **WF**, closely followed by **FF**, and finally

YF, suggesting that the folded β-hairpin populations change in this order. This, in turn, can be directly correlated to the strength of aromatic interactions and reflect upon the packing efficiency between the two ring systems. (ii) Unlike the observed abundance of Tyr-Phe pairs in proteins,[5b] interactions between these rings are seemingly less energetically favourable, compared to Phe-Phe and Trp-Phe interactions. Estimated ΔG^0_F (Fig. 3B) are in concurrence with these conclusions. Nevertheless, it has not escaped our notice that the non-equivalence of Phe7 $C^\delta H$ resonances is most prominent in **YF**. Whether weak interaction strengths between aromatic rings could promote alternate geometries in **YF**, is presently unknown. Nonetheless, the observed line broadening at lower temperatures in all the three peptides, due to slower rotational motion at χ_2, reflects coordinated ring flipping motion and an orientation-dependent stabilizing influence of the proximal aromatic ring.[9b]

We also examined the chemical shift dependence of the Phe7 $C^\delta H$ resonance to temperature (Fig. 5). At 303K, the extent of upfield shift follows the pattern **WF**>**FF**>**YF**. Upon lowering of temperature, the formation of stabilizing aromatic interactions results in further upfield shift of the $7C^\delta H$ protons. Beyond 270K (**FF**, **WF**) and 250K (**YF**), only a marginal change in the chemical shift is seen, suggesting that optimal ring geometries have been achieved for all three peptides below these temperatures. Furthermore, we do not observe the reported temperature dependence on solvophobic effect, which causes a downfield shift of the $7C^\delta H$ resonance at very low temperatures.[9b] Uniform line broadening of all backbone resonances at lower temperatures is consistent with increased solvent viscosity, thereby altering proton relaxation rates. We presume that differences in our observations and earlier reports may be due to key temperature-driven solvent contributions to peptide conformation and ring orientations.

Interestingly, when we extrapolate the Phe7 $C^\delta H$ chemical shift to predict values at higher temperatures (Fig. S9†), we observe that comparable $7C^\delta H$ chemical shifts may be obtained for all three peptides at ~375K. We assume that at this temperature, aromatic interactions are effectively inexistent. As the temperature is lowered, the rate of change in chemical shift of $7C^\delta H$ is highest in **WF**, suggesting that strong indole-benzyl interactions can be nucleated at temperatures that are not conducive for the formation of benzyl dimers or phenolic-benzyl interactions. It can also be argued that the rapid shift in $7C^\delta H$ from 375K to ~300K could be the result of strong shielding from the indole. However, other deterministic features including CSI, NOE intensities, ^3J and $\Delta G_0{}^F$ support the presence of stronger aromatic interactions in **WF**. Below ~270K, the rate of upfield shift of $7C^\delta H$ is comparable in **FF** and **WF**, suggesting that favourable contributions of an indole are no longer superior to a Phe ring. However, **YF** requires further lowering in temperature (~250K), reflecting weaker Tyr-Phe interactions.

We also see a prominent temperature dependent chemical shift change of two indole resonances in **WF** (Fig. 5). The $2C^\delta H$ shows a significant and unusual downfield shift upon lowering of temperature, while the $2C^{\varepsilon 3}H$ shows a marginal upfield movement. The former observation may be attributed to the hydrogen bond stabilization of the neighbouring $2N^{\varepsilon 1}H$.

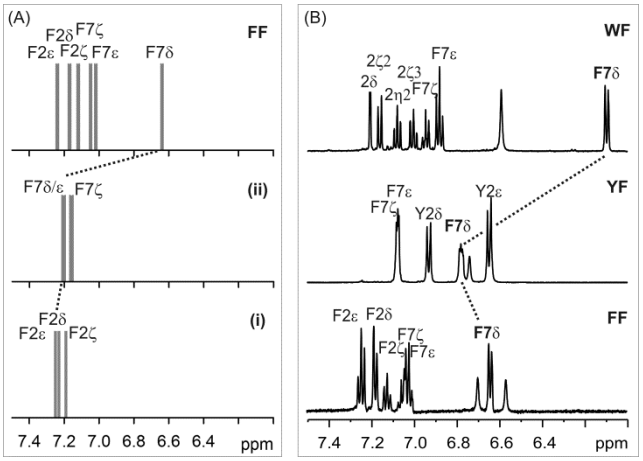

Fig. 4 Extent of benzyl ring shielding under the influence of the interacting partner. (A) Stick plot of Phe7 ring proton resonances, comparing the upfield shift of Phe7 $C^\delta H$ across three peptides, recorded in CD_3OH. (i) Boc-LFV-OCH_3,[9b] (ii) Boc-LVV-^{D}PG-LFV-OCH_3,[9b] (iii) **FF** (this study). (B) Partial expansions of 1D ^1H NMR spectra of **FF**, **YF** and **WF** in CD_3OH, comparing the dispersion and extent of upfield shift of aromatic resonance, particularly F7 $C^\delta H$, across the three peptides.

We however do not have convincing evidence for the unique behaviour of the $2C^{\varepsilon 3}H$. We speculate that at lower temperatures, alternative interaction geometries populated due to restricted χ_1 and χ_2 rotations may result in shielding of this resonance.

Neighbouring backbone resonances and anomalous ECD carry information on spatially proximal aromatics

The extent to which the chemical shift of a resonance is affected by aromatic interactions depends primarily on the electron density of the interacting ring (which is a function of the ring size) and on the occupancy (which depends on the number and strength of the interactions formed at each allowed ring orientation). When χ_1 is restricted by stabilization of one of the allowed geometries by strong local interactions, deviation of the geminal $C^\beta H$ proton chemical shifts of the aromatic amino acids from random coil values is observable, particularly for the ring undergoing shielding.[3g] A comparison of the $C^\beta H$ resonances of aromatic residue in position 2 with Phe7 (Fig. S10†), reveals a striking difference in the chemical shifts of Phe7 $C^\beta H$ resonances only in the peptide **WF**. Furthermore, the Phe7 $C^\alpha H$ also displays anomalous values that are not in line with the observed secondary structure (see Fig. 3A).

We examined the effect of substituting a bulky ring at position 2 on Phe7 $C^\alpha H$ chemical shifts (Fig. S11†) and CSI values (Fig. S5†), with temperature. We observe noticeable upfield shift only for Phe7 $C^\alpha H$ and $C^\beta H$, and the chemical shift change is most pronounced in **WF**. The change in $7C^\alpha H$ is linear between 220-320K, with a rate of change in chemical shift as follows: 5.1ppb/K (**FF**), 5.5ppb/K (**YF**) and 5.3ppb/K (**WF**). Our data indicates that at lower temperatures, greater ordering of the aromatic side chains occurs without substantial alteration of the β-hairpin population in all three peptides. Restricting dynamic motions around χ_1 and χ_2 of **YF** require maximum lowering of temperature. Tyr-Phe interactions are readily perturbed by the system energy, and therefore, its contribution to hairpin stabilization is indeed poorer.

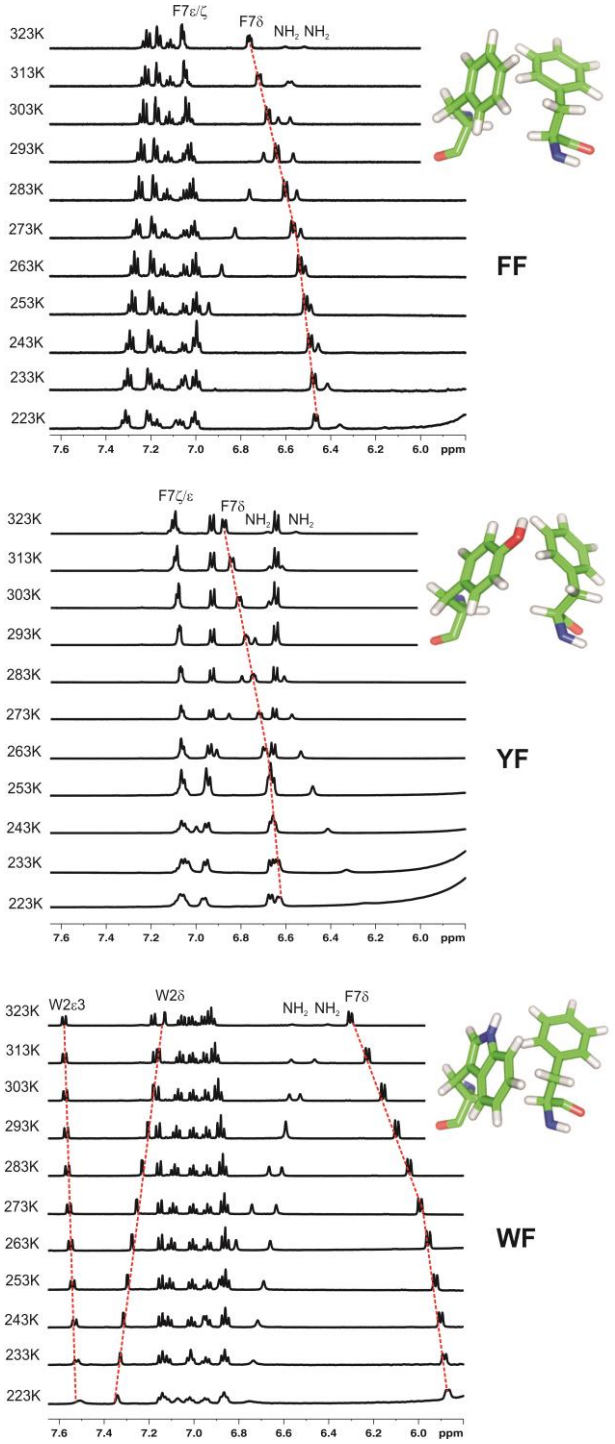

Fig. 5 Stack plots of 1D ^{1}H NMR spectra of aromatic resonances of **FF** (top), **YF** (middle) and **WF** (bottom), over the temperature range of 223K-323K, recorded at increments of 10K. Resonances that display a change in chemical shift with temperature are highlighted using dotted lines. Also shown as insets are the respective aromatic ring orientations, generated from the calculated NMR structures for each peptide, highlighting the FtE T-shaped side-chain interactions.

Furthermore, the observation of substantial contributions from aromatic interactions to the far-UV electronic circular dichroism (ECD) spectra also serves as qualitative indicators of strong ring interactions (Fig. S12†).[2h, 3g] **FF** displays two negative bands at ~195nm and ~210nm arising from Phe-Phe interactions.[23] Similarly, the spectrum for **YF** resembles the spectrum observed for Tyr-Tyr interactions,[2h] suggesting that the contributions of Phe to far-UV CD is surpassed by the influence of Tyr. Preponderance of strong aromatic contributions in **WF**, with a minor positive band at 228nm and negative maxima at ~200nm and ~210nm,[3g] is in line with our conclusions from NMR experiments.

Conclusions

Our systematic comparison of aromatic-Phe interactions, in attempts to understand their preferred interaction geometries and associated energy contributions to designed structural scaffolds, reveals that in the absence of bulk interactions, they preferentially associate in FtE T-shaped geometries. The major scaffold stabilization we observe in an amphipathic environment for this FtE geometry, is in the order **WF**>**FF**>**YF**, and contributes between 0.7-2kcal/mol to the folding free energy. While similar values have been obtained for aromatic interactions in aqueous systems,[2b, 3a, 3g] a direct comparison of our results with such studies is not possible. The interaction geometry is, however, conserved in both solvent systems. Similar FtE geometries are also observable in octapeptide hairpins bearing Phe2-Trp7 interactions (data not shown); however, such an interaction is anticipated to be less stabilizing than the Trp-Phe pair.[24]

Surprisingly, Phe-Phe self-association is stronger than its interaction with a strongly polar ring such as tyrosine, despite the observed abundance of the latter in proteins. Furthermore, we have recently demonstrated that Tyr-His interactions are also weak.[25] This indicates that in proteins, tyrosine is possibly involved in additional stabilizing interactions such as hydrogen bonding; electrostatic T-shaped interactions may therefore not necessarily be the major stabilizing contribution of this residue.

The contribution of the indole ring of tryptophan to β-hairpin stabilization is unique, since the lowered phi value of W2 in the peptide **WF** indicates that a Trp residue may not necessarily stabilize the hairpin backbone (Table 1). Several Trp residues could indeed cause distortion (twist) of the antiparallel sheet structure, as observed, for instance, in the Trpzip peptides,[3a] due to the low propensity of Trp for β-sheet structures.[21] However, strong electrostatic interactions, mediated by the indole ring, can result in overall structural stability.[26]

Is **WF** indeed better than **FF** in terms of overall strand stabilization? While all three aromatic pairs give rise to stably refolded beta-hairpin scaffolds, a Trp-Phe pair would unequivocally be the residues of choice to obtain highly stable structures even in very short sequences. However, structural stability is often achieved at the expense of function or unfavourable local distortions, as observed, for instance, in the case of the Trp-Trp pairs of GB1.[3e, 27] In such cases, a Trp-Phe or Trp-Trp interaction, both of which may induce strand twisting, can readily be substituted by a Phe-Phe pair, without a sizeable compromise on scaffold stability. Similar studies on whether such preferred interplay between aromatic pairs and backbone contributions to overall β-hairpin fold stability exists for Tyr and Trp, are anticipated to throw interesting insight on aromatic interactions.

Experimental Section

Peptide synthesis and purification

All peptides were synthesized using conventional solid phase Fmoc chemistry on a Rink Amide AM resin. Activation of the carboxyl group was achieved using HATU+DIPEA in dry DMF. Fmoc removal was carried out using 20% piperidine in dry DMF. After completion of synthesis, the peptides were simultaneously deprotected and cleaved from the resin using a cleavage cocktail comprising TFA (88): water (5): phenol (5): triisopropylsilane (2), and recovered using cold ether. All peptides were purified using HPLC on a C_{18} column using methanol-water gradients and checked using mass spectrometry and analytical HPLC†.

Structural characterization

NMR experiments were carried out on a Bruker Avance III 500MHz spectrometer (Bruker BioSpin GmbH) in CD_3OH with peptide concentrations of ~2-3mM. Unless otherwise specified, all data were acquired at 303K. 1D spectra were acquired using 32K data points and processed with a 0.3Hz line broadening. All 2D TOCSY and ROESY experiments were recorded in phase sensitive mode using standard pulse programs and excitation sculpting water suppression. 1024 and 256 data points were collected in the *f2* and *f1* dimensions, respectively. Mixing time of 80ms and 250ms were used for TOCSY and ROESY experiments, respectively. NMR data were processed using Topspin v3.0. Solvent-exposed amides were characterized by recording ^{1}H 1D spectra from 223K - 323K at an interval of 10K and the temperature coefficient was determined. All spectra were referenced using TMS (0ppm) or residual methanol peak (3.316ppm).

Structure calculation

All structure calculation was carried out using CYANA v2.1.[20] ^{D}Pro coordinates were added to the library. Upper distance restraint file was generated by assigning distance limits of 2.5Å, 3.5Å and 5Å to strong, medium and weak NOEs, respectively, and structures were calculated. This was refined by introducing 4 hydrogen bond constraints and 12 angle constraints. A total of 100 structures were calculated and dihedral angles for the 35 best structures were derived using PyMol[28] and MolMol.[29]

Free energy calculations

$C^{\alpha}H$ chemical shifts of residues 2, 3 and 6 were used to estimate equilibrium free energy of folding (ΔG^0_F), as reported.[2h] Random coil and β-sheet chemical shifts obtained from BMRB[30] were used to calculate the folded fractions, equilibrium populations (K_{eq}) and folding free energy, as reported earlier.[2h, 25]

Electronic circular dichroism measurements

Far-UV CD spectra were recorded in methanol on a JASCO J-815 CD spectropolarimeter (Jasco Inc., Japan) equipped with peltier control. Spectra were acquired between 200-300nm using scan speeds of 50nm/min at 0.5nm intervals, band width of 0.5nm, and averaged over 3 scans. Spectra were blank subtracted and smoothened. Plots were generated using SigmaPlot v11.0 (Systat Software).

Acknowledgements

This work is funded by intramural funds. K.M.M. is supported by a Research Fellowship from the University Grants Commission (UGC), Govt. of India. R.M. is a recipient of the Ramalingaswami fellowship from the Department of Biotechnology (DBT), Govt. of India.

Notes and references

[a] *Molecular Biophysics Laboratory, Department of Biological Sciences, Indian Institute of Science Education and Research, Bhopal, India. Fax: 91 755 4092392; Tel: 91 755 4092318; E-mail: maha@iiserb.ac.in*

† Electronic Supplementary Information (ESI) available: [Supporting Figures and Tables]. See DOI: 10.1039/b000000x/

1. (a) J. Fernandez-Recio, A. Vazquez, C. Civera, P. Sevilla and J. Sancho, *J. Mol. Biol.*, 1997, **267**, 184-197; (b) R. Bhattacharyya, U. Samanta and P. Chakrabarti, *Protein Eng.*, 2002, **15**, 91-100; (c) S. M. Butterfield, P. R. Patel and M. L. Waters, *J. Am. Chem. Soc.*, 2002, **124**, 9751-9755; (d) L. K. Tsou, C. D. Tatko and M. L. Waters, *J. Am. Chem. Soc.*, 2002, **124**, 14917-14921.
2. (a) A. J. Maynard, G. J. Sharman and M. S. Searle, *J. Am. Chem. Soc.*, 1998, **120**, 1996-2007; (b) C. D. Tatko and M. L. Waters, *J. Am. Chem. Soc.*, 2002, **124**, 9372-9373; (c) B. Ciani, M. Jourdan and M. S. Searle, *J. Am. Chem. Soc.*, 2003, **125**, 9038-9047; (d) C. D. Tatko and M. L. Waters, *Protein Sci.*, 2004, **13**, 2515-2522; (e) C. D. Tatko and M. L. Waters, *J. Am. Chem. Soc.*, 2004, **126**, 2028-2034; (f) R. S. Roy, H. N. Gopi, S. Raghothama, R. D. Gilardi, I. L. Karle and P. Balaram, *Biopolymers*, 2005, **80**, 787-799; (g) R. M. Hughes and M. L. Waters, *J. Am. Chem. Soc.*, 2006, **128**, 13586-13591; (h) R. Mahalakshmi, S. Raghothama and P. Balaram, *J. Am. Chem. Soc.*, 2006, **128**, 1125-1138.
3. (a) A. G. Cochran, N. J. Skelton and M. A. Starovasnik, *Proc. Natl. Acad. Sci. U. S. A.*, 2001, **98**, 5578-5583; (b) M. L. Waters, *Curr. Opin. Chem. Biol.*, 2002, **6**, 736-741; (c) S. E. Kiehna and M. L. Waters, *Protein Sci.*, 2003, **12**, 2657-2667; (d) R. Rai, S. Raghothama and P. Balaram, *J. Am. Chem. Soc.*, 2006, **128**, 2675-2681; (e) L. Eidenschink, B. L. Kier, K. N. Huggins and N. H. Andersen, *Proteins*, 2009, **75**, 308-322; (f) C. M. Santiveri and M. A. Jimenez, *Biopolymers*, 2010, **94**, 779-790; (g) L. Wu, D. McElheny, T. Takekiyo and T. A. Keiderling, *Biochemistry*, 2010, **49**, 4705-4714; (h) C. M. Santiveri, M. J. Perez de Vega, R. Gonzalez-Muniz and M. A. Jimenez, *Org. Biomol. Chem.*, 2011, **9**, 5487-5492.
4. Y. Mirassou, C. M. Santiveri, M. J. Perez de Vega, R. Gonzalez-Muniz and M. A. Jimenez, *ChemBioChem*, 2009, **10**, 902-910.
5. (a) R. Chelli, F. L. Gervasio, P. Procacci and V. Schettino, *J. Am. Chem. Soc.*, 2002, **124**, 6133-6143; (b) E. Lanzarotti, R. R. Biekofsky, D. A. Estrin, M. A. Marti and A. G. Turjanski, *J. Chem. Inf. Model.*, 2011, **51**, 1623-1633.
6. (a) M. L. Waters, *Biopolymers*, 2004, **76**, 435-445; (b) S. Aravinda, U. S. Raghavender, R. Rai, V. V. Harini, N. Shamala and P. Balaram, *Org. Biomol. Chem.*, 2013, **11**, 4220-4231.
7. G. B. McGaughey, M. Gagne and A. K. Rappe, *J. Biol. Chem.*, 1998, **273**, 15458-15463.
8. (a) S. K. Burley and G. A. Petsko, *Science*, 1985, **229**, 23-28; (b) T. Takekiyo, L. Wu, Y. Yoshimura, A. Shimizu and T. A. Keiderling, *Biochemistry*, 2009, **48**, 1543-1552.
9. (a) A. Rajagopal, S. Aravinda, S. Raghothama, N. Shamala and P. Balaram, *Biopolymers*, 2012, **98**, 185-194; (b) R. Sonti, R. Rai, S.

Ragothama and P. Balaram, *J. Phys. Chem. B*, 2012, **116**, 14207-14215.
10. S. Aravinda, N. Shamala, C. Das, A. Sriranjini, I. L. Karle and P. Balaram, *J. Am. Chem. Soc.*, 2003, **125**, 5308-5315.
11. J. Kyte and R. F. Doolittle, *J. Mol. Biol.*, 1982, **157**, 105-132.
12. (a) R. Wolfenden, L. Andersson, P. M. Cullis and C. C. Southgate, *Biochemistry*, 1981, **20**, 849-855; (b) G. D. Rose and R. Wolfenden, *Annu. Rev. Biophys. Biomol. Struct.*, 1993, **22**, 381-415.
13. J. Janin, *Nature*, 1979, **277**, 491-492.
14. S. Hwang, Q. Shao, H. Williams, C. Hilty and Y. Q. Gao, *J. Phys. Chem. B*, 2011, **115**, 6653-6660.
15. (a) I. L. Karle, C. Das and P. Balaram, *Proc. Natl. Acad. Sci. U. S. A.*, 2000, **97**, 3034-3037; (b) C. Das, S. C. Shankaramma and P. Balaram, *Chem. Eur. J.*, 2001, **7**, 840-847.
16. A. Sengupta, R. Mahalakshmi, N. Shamala and P. Balaram, *J. Pept. Res.*, 2005, **65**, 113-129.
17. R. Rai, S. Raghothama, R. Sridharan and P. Balaram, *Biopolymers*, 2006, **88**, 350-361.
18. N. H. Andersen, J. W. Neidigh, S. M. Harris, G. M. Lee, Z. H. Liu and H. Tong, *J. Am. Chem. Soc.*, 1997, **119**, 8547-8561.
19. R. Sonti, H. N. Gopi, U. Muddegowda, S. Ragothama and P. Balaram, *Chem. Eur. J.*, 2013, **19**, 5955-5965.
20. P. Guntert, *Methods Mol. Biol.*, 2004, **278**, 353-378.
21. E. Yurtsever, D. Yuret and B. Erman, *J Phys Chem A*, 2006, **110**, 13933-13938.
22. J. Singh and J. M. Thornton, *FEBS Lett.*, 1985, **191**, 1-6.
23. C. X. Zhao, P. L. Polavarapu, C. Das and P. Balaram, *J. Am. Chem. Soc.*, 2000, **122**, 8228-8231.
24. U. Samanta, D. Pal and P. Chakrabarti, *Acta Crystallogr. D Biol. Crystallogr.*, 1999, **55**, 1421-1427.
25. K. M. Makwana, S. Raghothama and R. Mahalakshmi, *Phys Chem Chem Phys*, 2013, **15**, 15321-15324.
26. A. G. Cochran, R. T. Tong, M. A. Starovasnik, E. J. Park, R. S. McDowell, J. E. Theaker and N. J. Skelton, *J. Am. Chem. Soc.*, 2001, **123**, 625-632.
27. (a) S. J. Russell, T. Blandl, N. J. Skelton and A. G. Cochran, *J. Am. Chem. Soc.*, 2003, **125**, 388-395; (b) M. Jager, M. Dendle, A. A. Fuller and J. W. Kelly, *Protein Sci.*, 2007, **16**, 2306-2313.
28. *The PyMOL Molecular Graphics System, Version 1.2r3pre, Schrödinger, LLC.*
29. R. Koradi, M. Billeter and K. Wuthrich, *J. Mol. Graph.*, 1996, **14**, 51-55, 29-32.
30. E. L. Ulrich, H. Akutsu, J. F. Doreleijers, Y. Harano, Y. E. Ioannidis, J. Lin, M. Livny, S. Mading, D. Maziuk, Z. Miller, E. Nakatani, C. F. Schulte, D. E. Tolmie, R. Kent Wenger, H. Yao and J. L. Markley, *Nucleic Acids Res.*, 2008, **36**, D402-408.

